Published in final edited form as:
Angiogenesis. 2014 January ; 17(1): 195–205. doi:10.1007/s10456-013-9388-z.

Proangiogenic microtemplated fibrin scaffolds containing aprotinin promote improved wound healing responses

Kassandra S. Thomson[1,2], **Sarah K. Dupras**[2], **Charles E. Murry**[1,2,3], **Marta Scatena**[1,2], and **Michael Regnier**[1,2,4]

[1]Department of Bioengineering, University of Washington, Seattle, WA 98195-5061

[2]Center for Cardiovascular Biology, Institute for Stem Cell and Regenerative Medicine, University of Washington, School of Medicine, Seattle, WA 98195-8050

[3]Departments of Pathology and Medicine/Cardiology, University of Washington, Seattle WA 98109

Abstract

Survival of tissue engineered constructs after implantation depends heavily on induction of a vascular response in host tissue, promoting a quick anastomosis of the cellular graft. Additionally, implanted constructs typically induce fibrous capsule formation, effectively preventing graft integration with host tissue. Previously we described the development of a high density microtemplated fibrin scaffold for cardiac tissue engineering applications with tunable degradation and mechanical properties which promoted seeded cell survival and organization *in vitro* (1). Scaffold degradation *in vitro* was controllable by addition of the serine protease inhibitor aprotinin and/or the fibrin cross-linker Factor XIII (FXIII). The goal of this study was to assess host tissue responses to these fibrin scaffold formulations by determining effects on scaffold degradation, angiogenic responses, and fibrous capsule formation in a subcutaneous implant model. Aprotinin significantly decreased scaffold degradation over 2 weeks of implantation. A significant increase in capillary infiltration of aprotinin implants was found after 1 and 2 weeks, with a significantly greater amount of capillaries reaching the interior of aprotinin scaffolds. Interestingly, after 2 weeks the aprotinin scaffolds had a significantly thinner, yet apparently more cellular fibrous capsule than unmodified scaffolds. These results indicate aprotinin not only inhibits fibrin scaffold degradation, but also induces significant responses in the host tissue. These included an angiogenic response resulting in increased vascularization of the scaffold material over a relatively short period of time. In addition, aprotinin release from scaffolds may reduce fibrous capsule formation, which could help promote improved integration of cell-seeded scaffolds with host tissue.

Introduction

An ideal scaffold for tissue engineering can support cell seeding and survival, promote tissue-level organization, have mechanical properties matching those of the target tissue, and induce a positive angiogenic response from host tissues (1–3). Implantation of any material initiates an inflammatory response from the host tissue, which is characterized by a coordinated and complex series of cellular events intended to heal the wound. The normal

[4]**Corresponding Author Information:** Michael Regnier, mregnier@u.washington.edu, Phone: 206-616-4325, 206-221-0504, Fax: 206-685-1457.

Conflict of Interest
The authors declare that they have no conflict of interest.

host response to constructs implanted for any significant amount of time is to deposit a fibrous capsule of collagen around the implant, known as the foreign body response, which can impede vascularization and integration with host tissue (4). Therefore, the development of biomaterials that can promote a more physiological healing response by decreasing fibrous capsule formation and inducing vascularization could improve the success of tissue engineered implants.

The ability to induce vascularization and anastomosis with the host tissue is critical for the survival of graft cells being delivered in tissue engineered constructs, especially for cells with high metabolic demand such as cardiomyocytes, and is a major factor in the extent of graft integration with the host tissue (3). A variety of scaffold materials have been investigated for their ability to promote vascular infiltration of implants, but a sufficient extent of graft vascularization is still one of the main challenges in tissue engineering (3, 5, 6). Recently we reported on microtemplated high density fibrin scaffolds for cardiac tissue engineering applications (1). Fibrinogen is a 340kDa protein which circulates in the bloodstream and which is arranged in three distinct domains (2 outer D-domains, and an inner E-domain). In the event of tissue injury, activated thrombin cleaves fibrinogen into fibrin monomers. These monomers autopolymerize into fibrin fibrils, which aggregate into a fibrin mesh and are further stabilized by factor XIII (FXIII) crosslinking. This crosslinked fibrin forms the major protein component of blood clots. Fibrin is naturally degraded by the serine protease plasmin, which is formed from its precursor plasminogen by the action of tissue plasminogen activator (t-PA) or urokinase-like plasminogen activator (uPA). Degradation of fibrin by plasmin leads to the formation of various fibrin degradation products (FDPs), including D-dimers, fibrin D-fragments, and fibrin E-fragments (7, 8). These FDPs have been shown to induce angiogenesis *in vivo* (7), and are naturally cleared by the body (2, 9).

Fibrin has been used by many groups as a hydrogel scaffolding material to deliver cells due to its natural cell adhesive properties, tunable architecture, and non-toxic degradation products (2, 10–14). Fibrin has been shown to improve survival of transplanted cells (15, 16), induce neovascularization and reduce infarct expansion when injected into ischemic myocardial tissue (14, 15, 17, 18). The need for a scaffolding material that can promote a favorable angiogenic response from the host tissue is significant in the field of tissue engineering, and fibrin is a promising biomaterial for this type of application. One issue with using fibrin for certain tissue engineering applications is the low mechanical strength of a fibrin hydrogel (2, 19). Increasing the density of fibrinogen used to form the fibrin gel has been shown to increase mechanical strength (2). In order to match the stiffness of some tissues (such as cardiac muscle), an extremely high concentration of fibrinogen is needed. However, these high concentration fibrin gels are too dense for cells to penetrate and are therefore not ideal for use as cell delivery vehicles.

To address this issue, our group developed a microtemplating technique for high density fibrin which allows fabrication of fibrin scaffolds with much higher stiffness than fibrin gels, while maintaining void space in the form of microchannels and an interconnected microporous network to promote high density cell-seeding and nutrient exchange within scaffolds (1). The addition of a high concentration of FXIII and aprotinin (a serine protease inhibitor), alone and in combination, were previously tested to determine their effects on scaffold stiffness and degradation *in vitro*. Significant differences were found in the rate of degradation between scaffold modification groups in these *in vitro* studies (1), which indicated the potential for scaffold modifications to alter the *in vivo* degradation profile of our microtemplated fibrin.

The main goal of this study was to assess whether different scaffold modifications would induce different tissue responses by evaluating these high density microtemplated fibrin scaffold formulations in a subcutaneous implant model. Parameters that were investigated include the rate of scaffold degradation, the extent of host angiogenic response to scaffolds, the distribution of infiltrating vasculature within implants, and the effects on fibrous capsule formation around scaffolds over a two week implantation period.

Materials & Methods

Fibrin scaffold construction

Scaffolds were constructed according to previously published methods (1). Briefly, optical fibers (Paradigm Optics, Vancouver, WA) with a 60μm diameter inner polycarbonate (PC) core and a 30μm thickness poly(methyl methacrylate) (PMMA) outer shell were bundled and sintered at 145°C overnight to form a solid PMMA matrix containing PC cores spaced 60μm apart. After sectioning into 1–3mm length disks and immobilizing the ends of the PC cores with cyanoacrylate, the PMMA matrix was selectively dissolved with xylene washes over 5 days. The resulting void space around the PC cores was filled with PMMA microbeads (27μm diameter, Microbeads, Skedsmokorset, Norway) via sonic sifting, and the beads were sintered in place at 180°C for 24h to obtain a pore neck diameter 50% of the bead diameter. This polymer template was infiltrated with a 200mg/mL fibrinogen solution (bovine fibrinogen Type 1-S, Sigma-Aldrich, St. Louis, MO; in 0.9% NaCl) via centrifugation. Thrombin solution (13.25U/mL thrombin, Sigma-Aldrich, St. Louis, MO; 8.3mM $CaCl_2$; DMEM, Gibco, Grand Island, NY) pre- warmed to 37°C was used to polymerize the fibrinogen into fibrin around the polymer template overnight at room temperature. The polymer template was dissolved with two 24 hour washes in a 90% dichloromethane/10% hexanes solution followed by a 24h acetone wash at room temperature. Scaffolds were treated with 100% ethanol rinses for 1 week before rehydration with a graded ethanol series into sterile phosphate-buffered saline (PBS).

Scaffold modifications

Additional cross-linking of fibrin scaffolds was achieved by adding human Factor XIII (FXIII, 100μg/mL, Innovative Research, Novi, MI) to the fibrinogen solution before centrifugation into polymer templates. Inhibition of scaffold degradation by proteases was tested by adding the serine protease inhibitor aprotinin (3000U/mL, Sigma-Aldrich, St. Louis, MO) to the fibrinogen solution. These scaffold modifications were tested alone and in combination with each other to determine their effects on *in vivo* degradation and tissue responses to the fibrin scaffolds.

Acellular scaffold subcutaneous implants

After rehydration and equilibration in sterile PBS, acellular fibrin scaffolds (unmodified, FXIII, aprotinin, and FXIII + aprotinin) were cut into 2mm diameter ×3mm length cylinders for subcutaneous implantation and kept in sterile PBS at 4°C until use. All animal procedures were conducted in accordance with the US National Institutes of Health Policy on Humane Care and Use of Laboratory Animals and were approved by the University of Washington (UW) Animal Care Committee. Rats were housed in the Department of Comparative Medicine at UW and cared for in accordance with the UW Institutional Animal Care and Use Committee (IACUC) procedures. Adult male Fischer 344 rats (200–300g) were anesthetized with isoflurane before implantation following previously described procedures by our group (20). Briefly, rats (n = 12) received 4 subcutaneous hindlimb implants (2 on each side), one from each scaffold modification group. Sterile scaffolds were implanted into subcutaneous pockets in the left and right hindlimb regions. Rats were euthanized via pentobarbital overdose (120–150 mg/kg) administered via IP injection at

endpoints of 7 and 14 days (n = 6 per time point), after which subcutaneous implants with an area of tissue surrounding the suture site were retrieved. This method of euthanasia is in accordance with recommendations of the Panel on Euthanasia of the American Veterinary Medical Association.

Sample preparation and histology

Subcutaneous implants were immediately immersion-fixed in Methyl Carnoy's fixative after retrieval. Samples were processed, embedded in paraffin, and sectioned (5μm) for histology. Cross-sections were cut from the center (midpoint sections) and both distal ends of samples (approximately 200–300μm apart), and serial sections were stained with Masson's trichrome, picrosirius red, and with immunohistochemical staining using methyl green as the nuclear counterstain. Immunostaining was performed with primary antibodies against rat endothelial cell antigen (RECA-1, mouse anti-rat (1:10), AbD Serotec, Raleigh, NC) and macrophage marker CD68 (mouse anti-rat (1:100), AbD Serotec, Raleigh, NC). Samples were then labeled with a biotinylated secondary antibody (horse anti-mouse (1:400), Vector, Burlingame, CA) and developed with DAB (Sigma-Aldrich, St. Louis, MO).

Histological analysis

Histological analysis of subcutaneous implants was performed using ImageJ analysis software v1.46 (NIH, Bethesda, MD, USA). All analyses were performed on midpoint and distal end sections (3–4 sections/sample) and then averaged for each sample unless otherwise noted. All samples were imaged and analyzed in a blinded fashion. The cross-sectional area of implant remaining was determined from Masson's trichrome staining. The density of RECA-1+ lumen structures (capillaries) was determined both within scaffold implants and in an area of tissue between the scaffold and the outer edge of the fibrous capsule on the skin side of implants, and normalized to area (mm^2). Only midpoint sections were used for analysis of capillary density in Day 14 samples due to the extent of scaffold degradation in these end sections. The percent area of CD68+ staining was determined by thresholding images of CD68 stained samples using ImageJ, and then averaging the percent positive area for 3 separate fields of equal size (at 20× magnification) within each scaffold section while avoiding the edges of the implants, as well as in an area of tissue between the scaffold and the outer edge of the fibrous capsule on the skin side of implants. Fibrous capsule thickness was determined from Masson's trichrome-stained sections by taking 4 measures of capsule thickness on the skin side of the implant in each section. Capsule location and thickness measurements were verified with picrosirius red-stained samples, both with brightfield and polarized light imaging using previously described protocols (21). In order to measure fibrous capsule cellularity, an area of capsule on the skin side of implants was analyzed for the total number of cells (all nuclei) and normalized to area (mm^2).

Vascular distribution analysis

To assess whether aprotinin scaffolds induced vascular infiltration to a greater extent than unmodified fibrin, a vascular distribution analysis was done on RECA-1 stained images using ImageJ and Adobe Illustrator. An outline of the remaining scaffold in cross-section was drawn in ImageJ and used to calculate the centroid. A vector outline of the remaining scaffold area was then re-drawn using Adobe Illustrator, and resized around the centroid to delineate three concentric rings, each one third of the distance between the centroid and the initial outline. The number of RECA-1+ capillaries within each ring was counted, and the percentage of total capillaries in each ring was calculated.

Statistical analysis

All values are reported as mean ± S.E.M. When comparing multiple scaffold modification groups, statistical significance from unmodified scaffolds was determined with a one-way ANOVA test using the Dunnett method. When comparing aprotinin and unmodified scaffold groups to each other, statistical significance was determined using a paired Student's t-test with $p < 0.05$ considered significant.

Results

Aprotinin decreases scaffold degradation *in vivo*

The cross-sectional area of implants remaining after 7 and 14 days of implantation was used to indicate extent of scaffold degradation in the subcutaneous implant model. No significant difference in cross-sectional area was found between scaffold groups at the one week time point, with the remaining scaffold areas averaging approximately 1.4–1.5mm^2 (cross-sectional area of implants on Day 0 was calculated to be 3.1mm^2). However, at the two week time point a significantly greater amount of scaffold was found for the groups containing aprotinin. While unmodified and FXIII scaffolds were almost completely degraded by this time (0.042 ± 0.01mm^2 and 0.010 ± 0.007 mm^2, respectively), aprotinin and FXIII + aprotinin scaffolds were significantly less degraded (0.30 ± 0.05 mm^2 and 0.25 ± 0.04 mm^2, respectively) (Figure 1a). Representative Masson's trichrome images of Day 14 unmodified and aprotinin scaffold midpoint sections are shown in Figure 1b–c.

Aprotinin scaffolds increase angiogenic response

To assess effects on host tissue angiogenic response to the four scaffold modification groups, samples were analyzed for total number of RECA-1+ capillaries per area of scaffold, as well as extent of macrophage infiltration (%CD68+ area). A significantly greater number of capillary lumen structures were found in aprotinin scaffolds after 7 days of implantation (200 ± 40 lumens/mm^2) as compared to any other scaffold group at this time point (36 ± 30 lumens/mm^2 for unmodified scaffolds, 27 ± 10 lumens/mm^2 for FXIII scaffolds, and 23 ± 10 lumens/mm^2 for FXIII + aprotinin scaffolds), as shown in Figure 2a. Representative images of the vascularization response in 7 day unmodified and aprotinin implants are shown in Figure 3. In Figure 3e red blood cells can be seen within the larger diameter capillaries in the scaffold channels. This occurred in approximately 50–75% of these vessels in each section, and in all sections in which these larger diameter capillaries were found (data not shown). The vascular density within scaffolds significantly increased by the 14 day time point, with a significantly greater number of RECA-1+ capillary structures in aprotinin scaffolds (1300 ± 100 lumens/mm^2) as compared to unmodified scaffolds (570 ± 300 lumens/mm^2), as shown in Figure 2b. To determine whether these differences might be attributed to a differing host response in the surrounding tissue, the number of capillaries in an area of tissue surrounding the scaffolds was also assessed. No significant differences in capillary density were found in the surrounding tissue at Day 7 (Figure 2c). Surprisingly, at the 14 day time point a significantly lower number of lumen structures per area were found in the tissue surrounding aprotinin scaffolds (3000 ± 100 lumens/mm^2) as compared to unmodified scaffolds (4000 ± 300 lumens/mm^2) (Figure 2d).

The percent area of CD68+ staining was determined for 7 day unmodified and aprotinin scaffold implants, both from the interior of the implant material (excluding edge regions) and in an area of tissue surrounding the implant. A significantly greater amount of CD68+ staining was found within aprotinin scaffold implants (8.6 ± 0.5% CD68+ area) as compared to unmodified scaffold implants (6.2 ± 0.3% CD68+ area) (Figure 4a). In contrast, a significantly lower amount of CD68+ staining was found in the surrounding tissue for aprotinin scaffold implants (27 ± 2% CD68+ area) as compared to unmodified scaffold

implants (36 ± 1% CD68+ area) (Figure 4b). Representative images of CD68+ staining in unmodified and aprotinin implants and the resulting threshold level used for analysis are shown in Figure 4c–f.

Aprotinin induces vascular infiltration of scaffolds

To assess whether aprotinin scaffolds were inducing lumen structure infiltration further into the interior regions of implants, a vascular distribution analysis was performed on Day 7 unmodified and aprotinin samples (Figure 5a). For midpoint sections, a significantly greater average number of capillary structures were found in the outer and middle rings of aprotinin scaffolds when compared with unmodified scaffolds (41 ± 20 lumens (outer ring) & 5.2 ± 3 lumens (middle ring) for aprotinin scaffolds; 3.0 ± 1 lumens (outer ring) & 0.0 ± 0 lumens (middle ring) for unmodified scaffolds) (Figure 5b). Representing these values as percentages of the total number of lumens found within the implants, approximately 72% of lumens were found in the outer ring, 20% in the middle ring, and 8% in the inner ring for midpoint sections of aprotinin scaffolds. For unmodified scaffolds, 100% of capillary lumen structures were found in the outer ring. In contrast to the results for midpoint sections, no significant differences in capillary distribution were found in distal end sections for unmodified and aprotinin scaffolds at this time point (Figure 5c).

Fibrous capsule thickness is reduced by aprotinin scaffolds

Fibrous capsule thickness was measured for unmodified and aprotinin scaffolds at the 7 and 14 day time points (Figure 6a) from trichrome stained sections, and results were confirmed with picrosirius red staining. No significant difference in capsule thickness was seen between unmodified and aprotinin scaffolds at the 7 day time point. However, after 14 days of implantation aprotinin scaffolds showed significantly thinner fibrous capsules (0.064 ± 0.003mm) when compared to unmodified scaffolds (0.11 ± 0.004mm). In addition, unmodified scaffold capsule thickness significantly increased from day 7 to day 14, while the capsule thickness surrounding aprotinin scaffolds significantly decreased between time points. Representative picrosirius red staining of 14 day unmodified and aprotinin scaffolds demonstrating the differences in fibrous capsule thickness are shown with both brightfield (Figure 6c–d) and polarized light imaging (Figure 6e–f).

Capsule cellularity was investigated by determining the total number of cell nuclei in a selected area of capsule on the skin side of implants for unmodified and aprotinin scaffold groups (Figure 6b). No significant difference was found in the number of cells per area of capsule for these two scaffold groups at the 7 day time point ($6.1 \times 10^4 \pm 0.6 \times 10^4$ cells/mm^2 for unmodified scaffolds, $5.4 \times 10^4 \pm 0.8 \times 10^4$ cells/mm^2 for aprotinin scaffolds). However, although not statistically significant, there appears to be a greater number of cells per area of capsule surrounding aprotinin implants after 14 days ($3.3 \times 10^4 \pm 0.8 \times 10^4$ cells/mm^2) as compared to unmodified scaffolds ($1.1 \times 10^4 \pm 0.07 \times 10^4$ cells/mm^2). Capsule cellularity for both of these scaffold groups decreased from 7 to 14 days.

Discussion

Aprotinin is a broad spectrum 6.5kDa competitive serine protease inhibitor naturally derved from bovine lung tissue, and has well-known anti-fibrinolytic properties as an inhibitor of plasmin (22–24). Due to this ability to prevent fibrin clot degradation aprotinin has been used as a haemostatic agent during cardiac surgical procedures (25, 26) and as a component of fibrin glues and tissue sealants (27–29). In addition, many groups have demonstrated slowed degradation of fibrin hydrogels with the addition of aprotinin to the culture media (23, 24, 30) or into the fibrin material itself (29, 31). Aprotinin was utilized to modify fibrin scaffold degradation properties *in vitro* in a recent study by our group, in which we

demonstrated its addition to high density microtemplated fibrin scaffolds was able to significantly increase scaffold stiffness retention when compared to unmodified fibrin scaffolds or scaffolds with additional FXIII crosslinking alone (1).

One of the goals of modifying our fibrin material was to try and extend the lifetime of the scaffold after implantation, as unmodified fibrin scaffolds were found to degrade very quickly both *in vitro* and *in vivo* (1). In this study, four different fibrin scaffold modification groups were evaluated in our subcutaneous implant model. The amount of scaffold cross-sectional area remaining was measured after 1 and 2 weeks of implantation, and the results showed significantly more scaffold area remaining after 14 days in both scaffold groups containing aprotinin. This follows with the well-established role of aprotinin as an inhibitor of fibrin degradation, and indicates that aprotinin can be loaded into the microtemplated fibrin, retains its function during scaffold processing procedures, and is subsequently released in active form into the surrounding tissue. The stability of the aprotinin molecule against many forms of denaturation is attributable to its highly compact tertiary protein structure (32, 33), which accounts for the retention of its protease inhibitor activity even after organic solvent processing of the scaffolds during template removal. Despite the significant reduction in scaffold degradation seen in the presence of aprotinin, there was still a large overall reduction in scaffold area over the 2 week implantation period. These fibrin scaffolds are intended for use as a degradable delivery vehicle for graft cells, and were therefore designed to have a target degradation time of approximately 2–4 weeks in order to balance early mechanical support of graft cells with the increasing deposition of new ECM as cells integrate with the host tissue. The results of this study indicate the addition of aprotinin promoted scaffold retention to fit within this desired time frame.

Previous studies have shown pore size can have a significant effect on the extent of vascular infiltration of biomaterial scaffolds, and observed the greatest extent of vascularization in scaffolds with an average pore size of 35μm (34). In addition, the natural degradation products of fibrin have been shown to promote angiogenesis (8, 35–37). We therefore expected our fibrin scaffolds would be able to elicit a vascular response from the host tissue even at the relatively early time point of 7 days, due to the 27μm diameter porous architecture and release of fibrin degradation products. Interestingly, aprotinin scaffolds induced a significantly greater average number of capillary structures infiltrating the microtemplated fibrin implants at both the 7 and 14 day time points compared to unmodified implants. Even at the relatively early time point of 7 days, evidence of red blood cells was found in the majority of large diameter capillaries within scaffold channels, suggesting these vessels are able to support blood flow within the fibrin scaffolds. Aprotinin scaffolds also induced vascularization further into the interior regions of implants than did unmodified scaffolds, as shown by the results of the concentric rings analysis on day 7 implants. It is possible that the pro-angiogenic effect of aprotinin results from the longer persistence of the pro-angiogenic scaffold architecture. Alternatively, aprotinin may have direct pro-angiogenic results in this system as well. Further studies will be required to resolve this point.

In support of a direct pro-angiogenic function, aprotinin has been shown to induce angiogenesis in a chicken embryo chorioallantoic membrane assay, as well as induce endothelial cell activation and migration *in vitro* (22, 38). One proposed mechanism by which it may promote angiogenesis is by the inhibition of angiostatin generation by platelets (38, 39). Angiostatin induces apoptosis in and inhibits migration of endothelial cells (39), and is formed by the auto-proteolysis of plasmin (38). As an inhibitor of serine proteases (including plasmin), aprotinin has been shown to inhibit angiostatin generation by platelets and subsequently induce an increased angiogenic response (38). Another mechanism by which aprotinin might be affecting the angiogenic response is by increasing levels of the

growth factor pleiotrophin, which directly induces endothelial cell migration (22). Aprotinin has been shown to increase levels of pleiotrophin both by inhibiting its degradation by plasmin and by inducing its expression via transcriptional activation of the pleiotrophin gene (22). Since aprotinin is a relatively small molecule that can freely diffuse out of lower density fibrin hydrogels (29), we hypothesized that in our high density fibrin constructs aprotinin molecules would be entrapped within the dense fibrin network and released as the scaffold was degraded. One effect observed in this study was that additional FXIII crosslinking prevented the increase in angiogenic response seen in the presence of aprotinin, as no increase in the number of infiltrating lumen structures was seen in scaffolds containing both aprotinin and FXIII compared to unmodified scaffolds at the 7 day time point. It is possible that the additional FXIII crosslinking affects the release of aprotinin within scaffolds, or that it alters the release of fibrin degradation products. These potential mechanisms are supported by the fact that the remaining scaffold area was not significantly different between aprotinin and FXIII + aprotinin scaffold groups, yet the angiogenic response within scaffolds was significantly different. The results of this study, along with recently published *in vitro* degradation data on these scaffold formulations, support our hypothesis (1).

When the macrophage response was investigated, a significantly greater amount of CD68+ staining was found within aprotinin implants as compared to unmodified scaffolds at the 7 day time point. Macrophages coordinate the foreign body response and induce the infiltration of other cell types into the wound, including fibroblasts and endothelial cells (40). Therefore, an increased amount of macrophage infiltration into aprotinin implants correlates with the increased vascularization response seen in this implant group. Interestingly, when the vascular and macrophage responses in the tissue surrounding implants were investigated, aprotinin implants showed significant decreases in these cell types as compared to unmodified scaffolds (decreased CD68+ area at 7 days, decreased RECA-1+ lumen structures at day 14). Additionally, aprotinin implants had significantly thinner (but apparently more cellular) fibrous capsules at the day 14 time point compared to unmodified scaffolds. These results indicate aprotinin release from the fibrin material may be affecting the inflammatory and wound healing responses to the scaffold implants.

As neutrophils and later monocytes/macrophages are recruited to the site of healing, they release both pro- (including TNF-α, IL-1, and IL-6) and anti-inflammatory (including IL-10) cytokines which coordinate the wound healing response (41, 42). Aprotinin has been shown to induce expression of anti-inflammatory cytokines, which in turn inhibit release of pro-inflammatory cytokines from both macrophages and neutrophils (41, 43). In addition, aprotinin inhibits expression of endothelial cell receptors for neutrophils (ICAM-1)(41, 43) and inhibits production of pro-inflammatory cytokines which attract neutrophils (44), and therefore decreases accumulation of these inflammatory cells at the site of wound healing. Previous studies by our collaborators showed an increase in anti-inflammatory macrophages (M2 phenotype) within and around microporous implants when compared to non-porous implants, and that this macrophage switch corresponded with an increased extent of porous implant vascularization (40). An increase in M2 macrophage phenotype has also been associated with improved tissue remodeling and host response to implanted scaffolds (45). One potential explanation for the results found in this study could be that aprotinin is inducing a differential macrophage phenotype profile, which would affect the overall cellular responses and remodeling in the tissue surrounding implants. Future studies will investigate the macrophage response to implanted constructs to determine if this type of macrophage polarization is occurring.

An interesting finding of this study was the decreased capsule thickness found for aprotinin implants at the 14 day time point when compared to unmodified scaffolds. While fibrin is

known to attract fibroblasts and stimulate their proliferation and collagen secretion during normal wound healing, fibrin sealants (which typically contain aprotinin) have been shown to decrease tissue fibrosis and scar formation *in vivo* (28). Transforming growth factor beta (TGF-β) is one of the main factors responsible for promoting fibroblast proliferation and subsequent collagen deposition by these cells during wound healing (28), and is produced by different cell types including macrophages and epithelial cells (46). Aprotinin has been shown to completely inhibit the activation of TGF-β, and therefore reduce tissue fibrosis and capsule formation *in vivo* (46, 47). Therefore, a potential explanation for the reduced fibrous capsule thickness observed surrounding our aprotinin implants is the interaction of aprotinin with TGF-β activation via this pathway, resulting in decreased collagen deposition by fibroblasts.

A potential limitation of this study design is that the four implant sites (2 per hindlimb) were the same for each animal, and the scaffold type in each implant location was the same across all animals. The blood supply to subcutaneous tissues has been shown to differ between forelimb and hindlimb locations (48), and perfusion of different muscles also differs (49). In this study, all implants were placed in the same region of the upper hindlimb subcutaneous tissue to normalize for differences in blood flow and perfusion in different limbs or regions of the hindlimb. Future studies in which the scaffold types are placed in multiple implant locations are needed to determine if the effects seen in this study vary with implant site.

In this study we have described the host tissue responses to different modifications of our high density microtemplated fibrin scaffolds. The addition of the protease inhibitor aprotinin significantly decreased implant degradation and significantly increased vascular and macrophage infiltration of scaffolds. Additionally, aprotinin release from scaffolds decreased the extent of inflammation in the surrounding tissue, and promoted the formation of a thinner and more cellular fibrous capsule. Future studies will further investigate the host cell responses to aprotinin scaffolds, and eventually determine their effect on cell-seeded scaffold integration with host tissues.

Acknowledgments

The authors sincerely thank Mandy Lund, Matt Coons, Veronica Muskheli and Elizabeth Gay for their assistance with histological sample preparations and analysis, and Marc Takeno and Alex Chen for their assistance with polarized light imaging. This work was supported by National Institutes of Health (NIH) grant R01HL064387 to MR, MS and CEM, and P01 HL094374, P01 GM081719, U01 HL100405, and R01 HL084642 to CEM.

References

1. Thomson KS, Korte FS, Giachelli CM, Ratner BD, Regnier M, Scatena M. Prevascularized Microtemplated Fibrin Scaffolds for Cardiac Tissue Engineering Applications. Tissue Eng Part A. 2013
2. Linnes MP, Ratner BD, Giachelli CM. A fibrinogen-based precision microporous scaffold for tissue engineering. Biomaterials. 2007; 28:5298. [PubMed: 17765302]
3. Naderi H, Matin MM, Bahrami AR. Review paper: critical issues in tissue engineering: biomaterials, cell sources, angiogenesis, and drug delivery systems. J Biomater Appl. 2011; 26:383. [PubMed: 21926148]
4. Anderson JM. Biological Responses to Materials. Annu Rev Mater Res. 2001; 31:81.
5. Cosson M, Debodinance P, Boukerrou M, Chauvet MP, Lobry P, Crépin G, Ego A. Mechanical properties of synthetic implants used in the repair of prolapse and urinary incontinence in women: which is the ideal material? Int Urogynecol J Pelvic Floor Dysfunct. 2003; 14:169. [PubMed: 12955338]

6. Kidd KR, Nagle RB, Williams SK. Angiogenesis and neovascularization associated with extracellular matrix-modified porous implants. J Biomed Mater Res. 2002; 59:366. [PubMed: 11745574]
7. Bootle-Wilbraham C, Tazzyman S, Thompson W, Stirk C, Lewis C. Fibrin fragment E stimulates the proliferation, migration and differentiation of human microvascular endothelial cells in vitro. Angiogenesis. 2001; 4:269. [PubMed: 12197472]
8. Ge M, Ryan TJ, Lum H, Malik AB. Fibrinogen degradation product fragment D increases endothelial monolayer permeability. Am J Physiol. 1991; 261:L283. [PubMed: 1928363]
9. Monroe DM, Hoffman M. What does it take to make the perfect clot? Arterioscler Thromb Vasc Biol. 2006; 26:41. [PubMed: 16254201]
10. Ahmed TA, Dare EV, Hincke M. Fibrin: A Versatile Scaffold for Tissue Engineering Applications. Tissue Eng Part B Rev. 2008; 14:199. [PubMed: 18544016]
11. Barsotti MC, Felice F, Balbarini A, Di Stefano R. Fibrin as a scaffold for cardiac tissue engineering. Biotechnol Appl Biochem. 2011; 58:301. [PubMed: 21995533]
12. Chen X, Aledia AS, Ghajar CM, Griffith CK, Putnam AJ, Hughes CC, George SC. Prevascularization of a fibrin-based tissue construct accelerates the formation of functional anastomosis with host vasculature. Tissue Eng Part A. 2009; 15:1363. [PubMed: 18976155]
13. Giraud MN, Ayuni E, Cook S, Siepe M, Carrel TP, Tevaearai HT. Hydrogel-based engineered skeletal muscle grafts normalize heart function early after myocardial infarction. Artif Organs. 2008; 32:692. [PubMed: 18684206]
14. Ryu JH, Kim IK, Cho SW, Cho MC, Hwang KK, Piao H, Piao S, Lim SH, Hong YS, Choi CY, Yoo KJ, Kim BS. Implantation of bone marrow mononuclear cells using injectable fibrin matrix enhances neovascularization in infarcted myocardium. Biomaterials. 2005; 26:319. [PubMed: 15262474]
15. Christman KL, Fok HH, Sievers RE, Fang Q, Lee RJ. Fibrin glue alone and skeletal myoblasts in a fibrin scaffold preserve cardiac function after myocardial infarction. Tissue Eng. 2004; 10:403. [PubMed: 15165457]
16. Christman KL, Vardanian AJ, Fang Q, Sievers RE, Fok HH, Lee RJ. Injectable fibrin scaffold improves cell transplant survival, reduces infarct expansion, and induces neovasculature formation in ischemic myocardium. Journal of the American College of Cardiology. 2004; 44:654. [PubMed: 15358036]
17. Chekanov V, Akhtar M, Tchekanov G, Dangas G, Shehzad MZ, Tio F, Adamian M, Colombo A, Roubin G, Leon MB, Moses JW, Kipshidze NN. Transplantation of autologous endothelial cells induces angiogenesis. Pacing Clin Electrophysiol. 2003; 26:496.
18. Huang YC, Khait L, Birla RK. Contractile three-dimensional bioengineered heart muscle for myocardial regeneration. J Biomed Mater Res A. 2007; 80:719.
19. Jockenhoevel S, Zund G, Hoerstrup SP, Chalabi K, Sachweh JS, Demircan L, Messmer BJ, Turina M. Fibrin gel -- advantages of a new scaffold in cardiovascular tissue engineering. Eur J Cardiothorac Surg. 2001; 19:424. [PubMed: 11306307]
20. Stevens K, Kreutziger K, Dupras S, Korte F, Regnier M, Muskheli V, Nourse M, Bendixen K, Reinecke H, Murry C. Physiological function and transplantation of scaffold-free and vascularized human cardiac muscle tissue. Proc Natl Acad Sci U S A. 2009; 106:16568.
21. Tulloch NL, Muskheli V, Razumova MV, Korte FS, Regnier M, Hauch KD, Pabon L, Reinecke H, Murry CE. Growth of engineered human myocardium with mechanical loading and vascular coculture. Circ Res. 2011; 109:47. [PubMed: 21597009]
22. Koutsioumpa M, Hatziapostolou M, Mikelis C, Koolwijk P, Papadimitriou E. Aprotinin stimulates angiogenesis and human endothelial cell migration through the growth factor pleiotrophin and its receptor protein tyrosine phosphatase beta/zeta. Eur J Pharmacol. 2009; 602:245. [PubMed: 19059395]
23. Cholewinski E, Dietrich M, Flanagan TC, Schmitz-Rode T, Jockenhoevel S. Tranexamic acid-- an alternative to aprotinin in fibrin-based cardiovascular tissue engineering. Tissue Eng Part A. 2009; 15:3645. [PubMed: 19496679]

24. Ahmed TA, Griffith M, Hincke M. Characterization and inhibition of fibrin hydrogel-degrading enzymes during development of tissue engineering scaffolds. Tissue Eng. 2007; 13:1469. [PubMed: 17518706]
25. McEvoy MD, Reeves ST, Reves JG, Spinale FG. Aprotinin in cardiac surgery: a review of conventional and novel mechanisms of action. Anesth Analg. 2007; 105:949. [PubMed: 17898372]
26. Bull DA, Maurer J. Aprotinin and preservation of myocardial function after ischemia-reperfusion injury. Ann Thorac Surg. 2003; 75:S735.
27. Hickerson WL, Nur I, Meidler R. A comparison of the mechanical, kinetic, and biochemical properties of fibrin clots formed with two different fibrin sealants. Blood Coagul Fibrinolysis. 2011; 22:19. [PubMed: 21150581]
28. Buser Z, Kuelling F, Liu J, Liebenberg E, Thorne KJ, Coughlin D, Lotz JC. Biological and biomechanical effects of fibrin injection into porcine intervertebral discs. Spine (Phila Pa 1976). 2011; 36:E1201. [PubMed: 21325992]
29. Lorentz KM, Kontos S, Frey P, Hubbell JA. Engineered aprotinin for improved stability of fibrin biomaterials. Biomaterials. 2011; 32:430. [PubMed: 20864171]
30. Ye Q, Zünd G, Benedikt P, Jockenhoevel S, Hoerstrup SP, Sakyama S, Hubbell JA, Turina M. Fibrin gel as a three dimensional matrix in cardiovascular tissue engineering. Eur J Cardiothorac Surg. 2000; 17:587. [PubMed: 10814924]
31. Smith JD, Chen A, Ernst LA, Waggoner AS, Campbell PG. Immobilization of aprotinin to fibrinogen as a novel method for controlling degradation of fibrin gels. Bioconjug Chem. 2007; 18:695. [PubMed: 17432824]
32. Fritz H, Wunderer G. Biochemistry and applications of aprotinin, the kallikrein inhibitor from bovine organs. Arzneimittelforschung. 1983; 33:479. [PubMed: 6191764]
33. Carmona P, Molina M, Rodríguez-Casado A. Raman study of the thermal behaviour and conformational stability of basic pancreatic trypsin inhibitor. Eur Biophys J. 2003; 32:137.
34. Bryers JD, Giachelli CM, Ratner BD. Engineering biomaterials to integrate and heal: the biocompatibility paradigm shifts. Biotechnol Bioeng. 2012; 109:1898. [PubMed: 22592568]
35. Thompson WD, Smith EB, Stirk CM, Marshall FI, Stout AJ, Kocchar A. Angiogenic activity of fibrin degradation products is located in fibrin fragment E. J Pathol. 1992; 168:47. [PubMed: 1280677]
36. Dvorak HF, Harvey VS, Estrella P, Brown LF, McDonagh J, Dvorak AM. Fibrin containing gels induce angiogenesis. Implications for tumor stroma generation and wound healing. Lab Invest. 1987; 57:673. [PubMed: 2447383]
37. van Hinsbergh VW, Collen A, Koolwijk P. Role of fibrin matrix in angiogenesis. Ann N Y Acad Sci. 2001; 936:426. [PubMed: 11460496]
38. Jurasz P, Santos-Martinez MJ, Radomska A, Radomski MW. Generation of platelet angiostatin mediated by urokinase plasminogen activator: effects on angiogenesis. J Thromb Haemost. 2006; 4:1095. [PubMed: 16689764]
39. Radziwon-Balicka A, Moncada de la Rosa C, Zielnik B, Doroszko A, Jurasz P. Temporal and pharmacological characterization of angiostatin release and generation by human platelets: implications for endothelial cell migration. PLoS One. 2013; 8:e59281. [PubMed: 23555012]
40. Madden LR, Mortisen DJ, Sussman EM, Dupras SK, Fugate JA, Cuy JL, Hauch KD, Laflamme MA, Murry CE, Ratner BD. Proangiogenic scaffolds as functional templates for cardiac tissue engineering. Proc Natl Acad Sci U S A. 2010; 107:15211. [PubMed: 20696917]
41. Hill GE, Diego RP, Stammers AH, Huffman SM, Pohorecki R. Aprotinin enhances the endogenous release of interleukin-10 after cardiac operations. Ann Thorac Surg. 1998; 65:66. [PubMed: 9456097]
42. McEvoy MD, Taylor AG, Zavadzkas JA, Mains IM, Ford RL, Stroud RE, Jeffords LB, Beck CU, Reeves ST, Spinale FG. Aprotinin exerts differential and dose-dependent effects on myocardial contractility, oxidative stress, and cytokine release after ischemia-reperfusion. Ann Thorac Surg. 2008; 86:568. [PubMed: 18640335]

43. Asimakopoulos G, Lidington EA, Mason J, Haskard DO, Taylor KM, Landis RC. Effect of aprotinin on endothelial cell activation. J Thorac Cardiovasc Surg. 2001; 122:123. [PubMed: 11436044]
44. Hill GE, Pohorecki R, Alonso A, Rennard SI, Robbins RA. Aprotinin reduces interleukin-8 production and lung neutrophil accumulation after cardiopulmonary bypass. Anesth Analg. 1996; 83:696. [PubMed: 8831305]
45. Brown BN, Valentin JE, Stewart-Akers AM, McCabe GP, Badylak SF. Macrophage phenotype and remodeling outcomes in response to biologic scaffolds with and without a cellular component. Biomaterials. 2009; 30:1482. [PubMed: 19121538]
46. Lee CG, Homer RJ, Zhu Z, Lanone S, Wang X, Koteliansky V, Shipley JM, Gotwals P, Noble P, Chen Q, Senior RM, Elias JA. Interleukin-13 induces tissue fibrosis by selectively stimulating and activating transforming growth factor beta(1). J Exp Med. 2001; 194:809. [PubMed: 11560996]
47. Rolfe, B.; Mooney, J.; Zhange, B.; Jahnke, S.; Le, S-J.; Chau, Y-Q.; Huang, Q.; Wang, H.; Campbell, G.; Campbell, J. The Fibrotic Response to Implanted Biomaterials: Implications for Tissue Engineering, Regenerative Medicine and Tissue Engineering. Eberli, D., editor. 2011.
48. Obokata H, Yamato M, Tsuneda S, Okano T. Reproducible subcutaneous transplantation of cell sheets into recipient mice. Nat Protoc. 2011; 6:1053. [PubMed: 21720318]
49. Lindbom L, Arfors KE. Non-homogeneous blood flow distribution in the rabbit tenuissimus muscle. Differential control of total blood flow and capillary perfusion. Acta Physiol Scand. 1984; 122:225. [PubMed: 6516877]

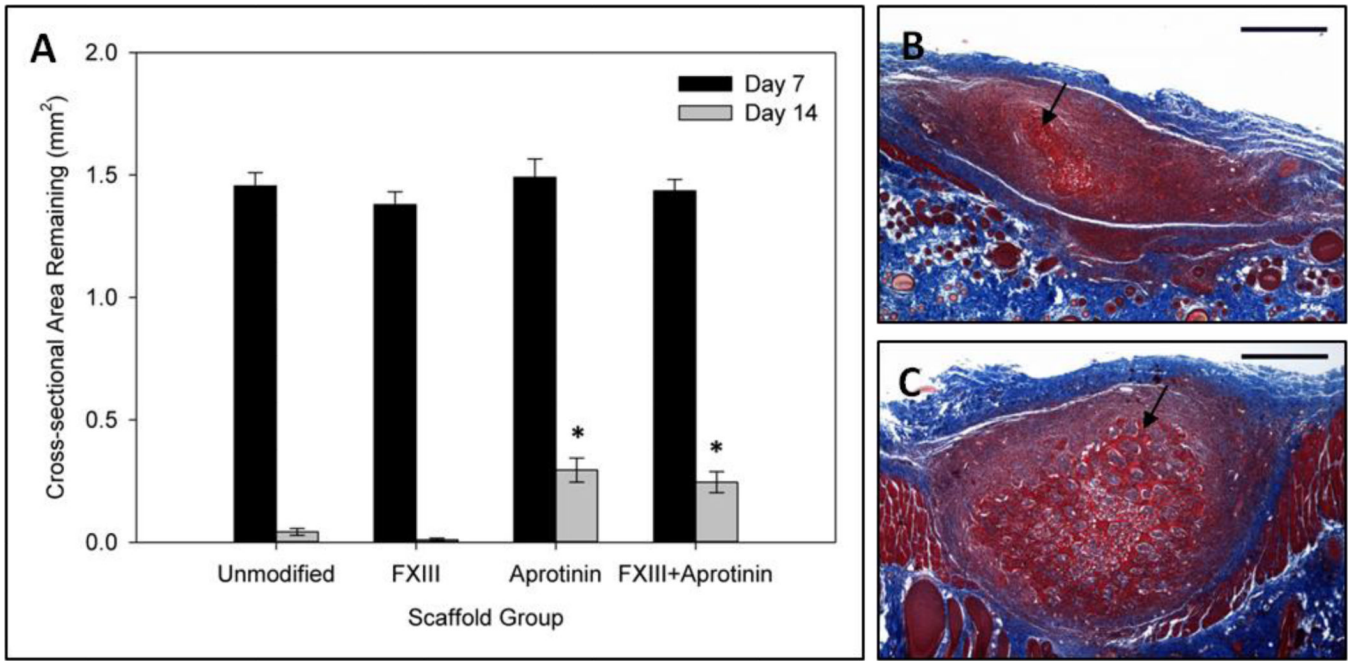

Fig. 1.

Degradation of scaffold formulations *in vivo*. **(a)** Cross-sectional area of scaffolds remaining after 7 & 14 days of subcutaneous implantation. Cross-sectional area of scaffolds at the time of implantation (Day 0) estimated as 3.1mm^2. Representative Masson's trichrome images for day 14 **(b)** unmodified scaffolds and **(c)** aprotinin scaffolds demonstrating the extent of scaffold degradation. Black arrows indicate fibrin scaffold material. ***** Indicates statistical significance from day 14 unmodified scaffolds (Student's t-test, $p < 0.05$). Scale bars = 500μm.

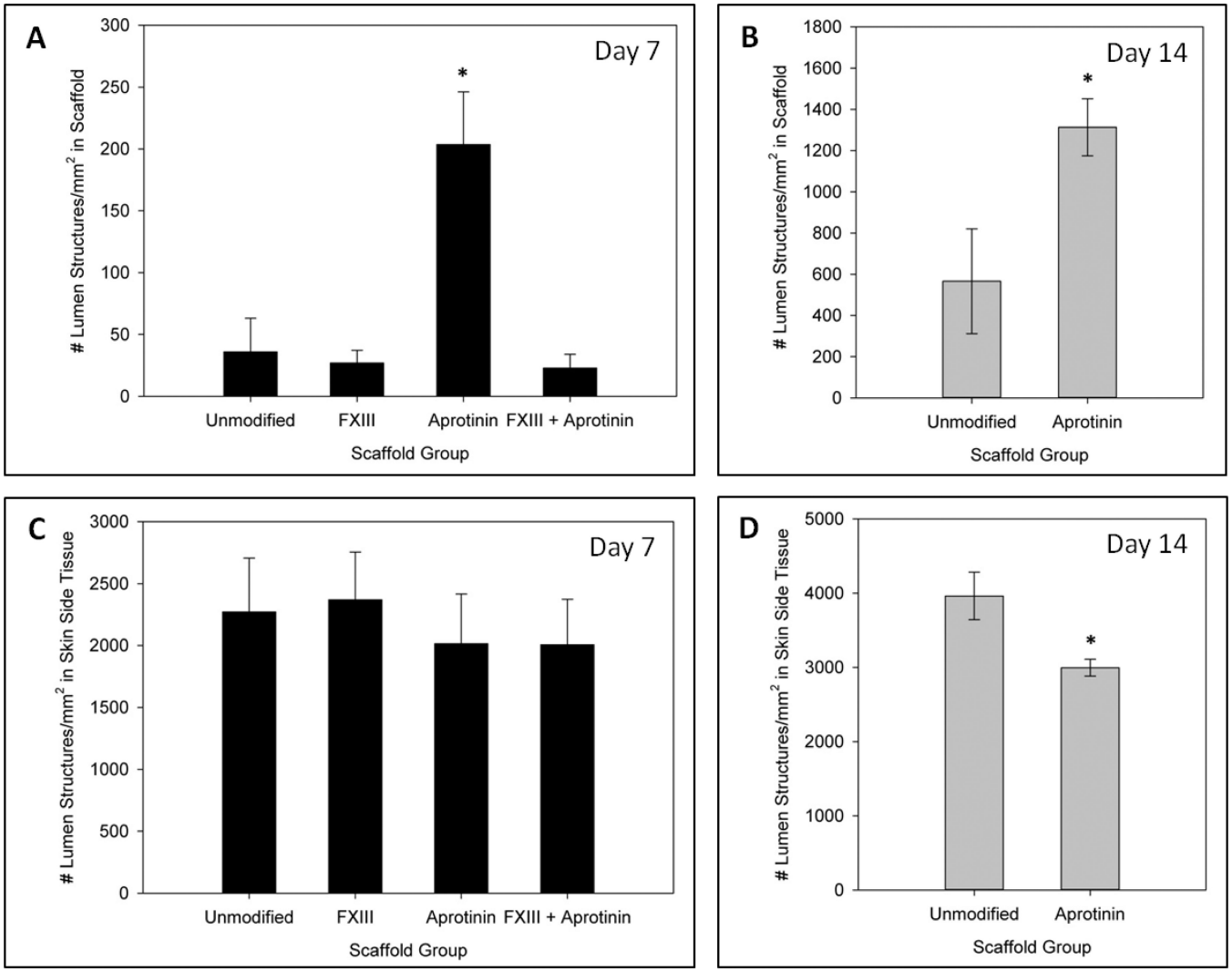

Fig. 2.

Induction of vascularization response by fibrin scaffold formulations. Average number of RECA-1+ lumen structures/mm^2 within scaffolds at **(a)** 7 days and **(b)** 14 days post-implantation. Average number of RECA-1+ lumen structures/mm^2 in an area of surrounding tissue on the skin side of implants at **(c)** 7 days and **(d)** 14 days post-implantation. ***** Indicates statistical significance from unmodified scaffolds (Student's t-test, $p < 0.05$).

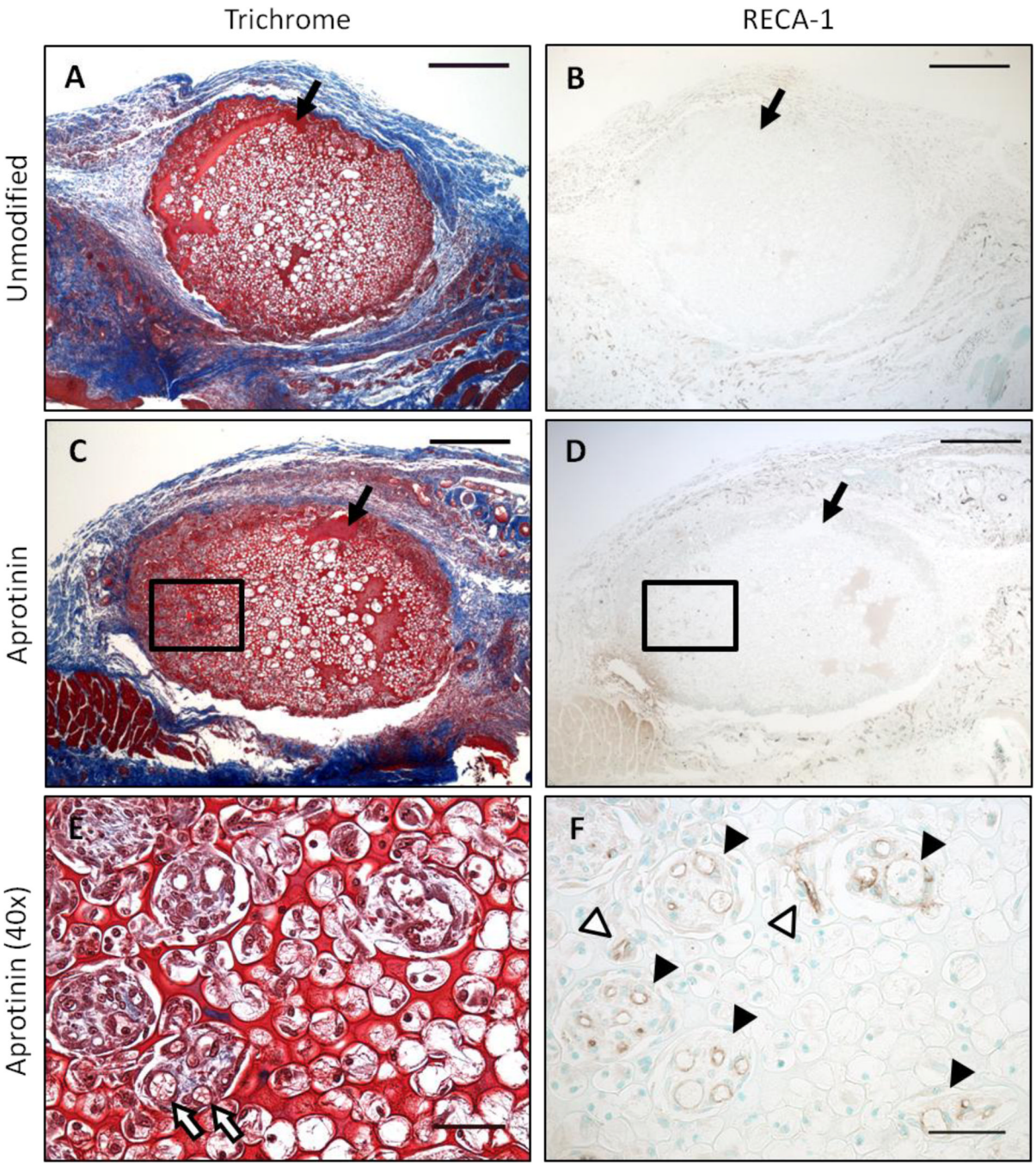

Fig. 3.

Vascularization response to implanted scaffolds. Representative images of **(a & b)** unmodified and **(c–f)** aprotinin scaffold implants after 7 days of implantation. **(a, c, & e)** Masson's trichrome staining with **(b, d, & f)** RECA-1+ staining of a consecutive section. Outlined areas in **(c)** and **(d)** are shown at higher magnification in **(e)** and **(f)**, respectively. Black arrows indicate fibrin material, white arrows indicate red blood cells within lumen structures, black arrowheads indicate RECA-1+ lumen structures in scaffold channels, white arrowheads indicate RECA-1+ lumen structures in scaffold pores. Scale bars in **(a–d)** = 500μm. Scale bars in **(e)** and **(f)** = 50μm.

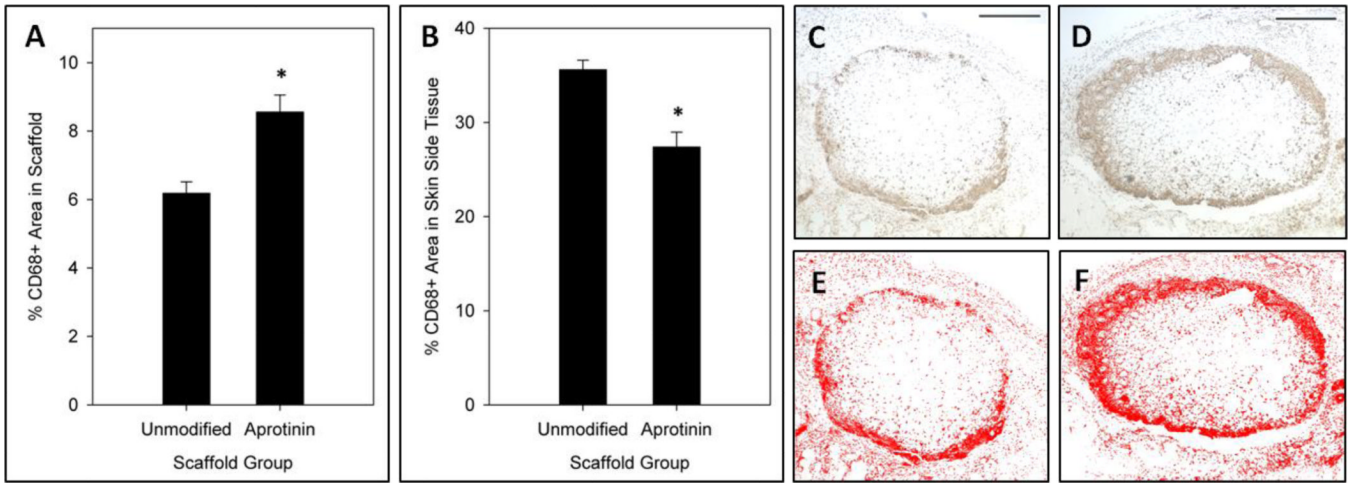

Fig. 4.

Macrophage response to 7 day scaffold implants. %CD68+ area **(a)** within scaffolds and **(b)** in an area of surrounding tissue on the skin side of implants. Representative CD68+ stained **(c)** unmodified and **(d)** aprotinin scaffolds, with corresponding threshold analysis images **(e & f)**. * Indicates statistical significance from unmodified scaffolds (Student's t-test, $p < 0.05$). Scale bars = 500μm.

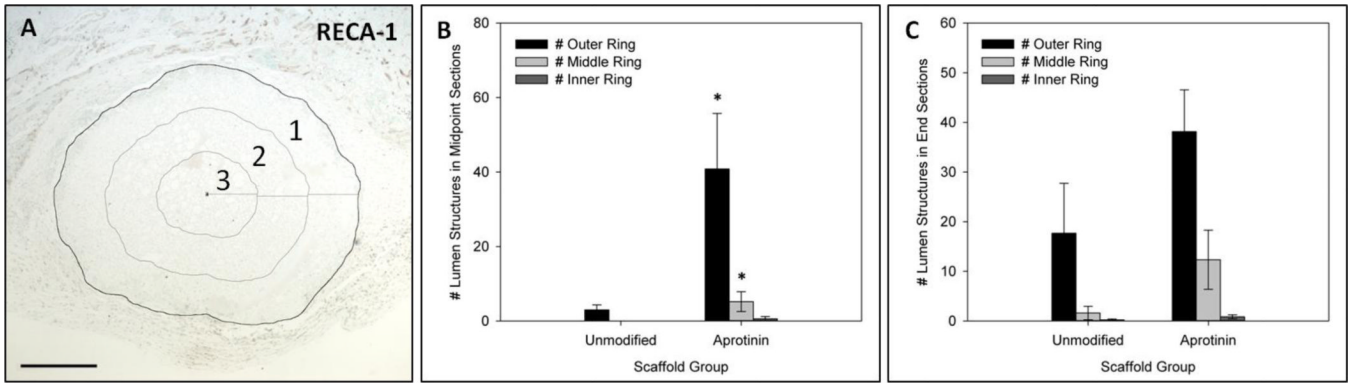

Fig. 5.

Concentric rings analysis to determine vascular distribution within 7 day implants. **(a)** Representative image showing concentric rings and centroid used for analysis. 1 = Outer ring; 2 = Middle ring; 3 = Inner ring. Average number of RECA-1+ lumen structures within each ring for unmodified and aprotinin scaffolds in **(b)** midpoint sections and **(c)** distal end sections. ***** Indicates statistical significance from corresponding ring in unmodified scaffolds (Student's t-test, $p < 0.05$). Scale bar = 500μm.

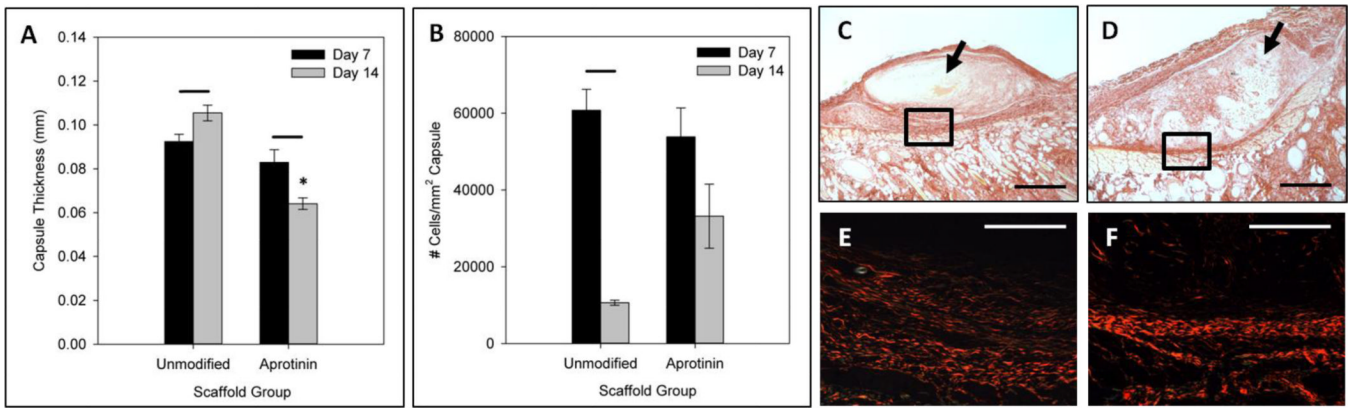

Fig. 6.

Fibrous capsule analysis of unmodified and aprotinin scaffold implants. **(a)** Average fibrous capsule thickness measured for scaffold groups at 7 and 14 days. **(b)** Average number of cells/mm^2 of capsule for 7 and 14 day implants. ***** Indicates statistical significance from 14 day unmodified scaffolds, bars indicate statistical significance from previous time point within a group (Student's t-test, $p < 0.05$). Representative brightfield images of picrosirius red staining of 14 day **(c)** unmodified scaffolds and **(d)** aprotinin scaffolds. Polarized light images of outlined areas in **(c)** and **(d)** are shown in **(e)** and **(f)**, respectively. Scale bars in **(c)** and **(d)** = 500μm, in **(e)** and **(f)** = 200μm.